

Preservation of heteronuclear multiple-quantum coherences in NMR by double-resonance irradiation

Mariachiara Verde,¹ Simone Ulzega,¹ Fabien Ferrage,^{2,a)} and Geoffrey Bodenhausen^{1,2}

¹*Institut des Sciences et Ingénierie Chimiques, Ecole Polytechnique Fédérale de Lausanne, 1015 Lausanne, Switzerland*

²*Département de Chimie, Ecole Normale Supérieure, associé au CNRS, 24 rue Lhomond, 75231 Paris Cedex 05, France*

(Received 6 August 2008; accepted 24 December 2008; published online 20 February 2009)

A heteronuclear double-resonance (HDR) method based on MLEV-32 or WALTZ-32 pulse sequences has been designed for the investigation of relaxation of heteronuclear multiple-quantum (MQ) coherences. The theoretical analysis of this technique uses average Hamiltonian theory (AHT) to treat the effects of coherent evolution associated with scalar couplings, offsets, and inhomogeneous radiofrequency (rf) fields during the pulse sequence. Under most conditions, the dynamics of the MQ coherences during the HDR sequence is not affected by rf inhomogeneities and scalar couplings for offsets as large as the nutation frequency. The predictions drawn from AHT are supported by numerical simulations and experiments. © 2009 American Institute of Physics. [DOI: 10.1063/1.3072559]

I. INTRODUCTION

Nuclear magnetic resonance (NMR) spectroscopy offers many ways to investigate dynamic properties of molecules. A wide variety of experimental techniques can probe molecular dynamics on time scales that range from 10^{-12} to 10^3 s.^{1,2} Many biological processes, such as protein folding, ligand binding, allosteric effects, and enzyme catalysis, involve conformational motions that occur on a microsecond to millisecond time scale. Conformational motions can give rise to chemical exchange contributions to relaxation. The two most popular NMR methods used to study these effects are Carr–Purcell–Meiboom–Gill (CPMG) echo trains^{3–6} and $R_{1\rho}$ spin-lock relaxation dispersion experiments.^{7–11} CPMG experiments are suited for the investigation of conformational exchange processes occurring on a millisecond time scale.^{12–15} In $R_{1\rho}$ experiments a radiofrequency (rf) field of amplitude ω_1 is applied in order to lock the magnetization in the rotating frame along an effective field $\omega_{\text{eff}} = \sqrt{\Omega^2 + \omega_1^2}$, where Ω is the offset from the carrier frequency. Such $R_{1\rho}$ experiments can probe chemical exchange processes on time scales ranging from milliseconds down to approximately $10 \mu\text{s}$.^{11,16,17} The past few years have seen significant advances in the developments of both methods for the characterization of dynamics in proteins.^{1,2,10,11} The reduced contribution of chemical exchange to relaxation rates under a spin lock has also been employed to obtain more precise and accurate NMR data.^{18,19}

CPMG and $R_{1\rho}$ studies of the relaxation rates of single quantum (SQ) coherences can be complemented by multiple-quantum coherence (MQC) experiments, which can provide information whether two spins (typically ^{15}N and ^1H nuclei)

are affected simultaneously by chemical exchange.^{20–24} In particular, heteronuclear MQC CPMG experiments have provided measurements of exchange rates and chemical shift differences between exchanging sites.^{22–24} So far, $R_{1\rho}$ experiments have been applied only to the study of SQ relaxation processes.

In heteronuclear systems, correlated chemical exchange, i.e., an exchange process which affects two nuclei simultaneously, gives rise to cross-relaxation between MQ coherences $2I_xS_x$ and $2I_yS_y$. The simultaneous application of two continuous-wave rf fields to both nuclei, for instance, along the x axes of the doubly rotating frame, allows one to lock a MQ coherence $2I_xS_x$ while $2I_yS_y$ nutates about the rf fields. Since unavoidable rf inhomogeneities will lead to partial dephasing of $2I_yS_y$, the observation of cross-relaxation between the two operators $2I_xS_x$ and $2I_yS_y$ becomes impractical under such conditions. Ideally, one should simultaneously preserve all coherences in the MQC subspace, i.e., $2I_xS_x$, $2I_xS_y$, $2I_yS_x$, and $2I_yS_y$, so that the interconversion between these operators can only arise through cross-relaxation.

We introduce a new method designed to effectively preserve all relevant MQ coherences simultaneously. This method can be employed to extend the scope of $R_{1\rho}$ experiments from SQ to MQ coherences and give access to dynamic processes that occur on time scales that are shorter than those accessible to CPMG experiments. This new method comprises a windowless sequence of rf pulses applied simultaneously to both spins I and S . The sequence is based on supercycles which are built on combinations of composite inversion pulses R and their phase-inverted counterparts \bar{R} . These supercycles constitute the basis of the well-known MLEV and WALTZ decoupling schemes.^{25–29} We have applied similar schemes in *double-resonance mode*, i.e., to both spins simultaneously. We shall refer to our schemes

^{a)}Electronic mail: fabien.ferrage@ens.fr.

as heteronuclear double resonance (HDR). In this paper, we consider only coherent spin dynamics. The effects of relaxation and chemical exchange will be treated elsewhere. In Secs. II and III we apply average Hamiltonian theory (AHT) to treat coherent effects and inhomogeneities of the rf fields. We present the results of simulations and experiments in Secs. IV and V.

II. COHERENT EVOLUTION: AVERAGE HAMILTONIAN THEORY

A. Introduction

Throughout this paper, we consider an isolated heteronuclear system comprising two scalar-coupled spins $I=1/2$ and $S=1/2$, such as $^{15}\text{N}-^1\text{H}^{\text{N}}$ pairs in perdeuterated proteins which are enriched uniformly with ^{15}N (but not ^{13}C).

The Hamiltonian in the laboratory frame (LF) that describes a scalar-coupled heteronuclear two-spin system under the effect of two rf fields can be written as

$$H^{(\text{LF})}(\tau) = H_0^{(\text{LF})} + H_{\text{rf}}^{(\text{LF})}(\tau), \quad (1)$$

with

$$H_0^{(\text{LF})} = \omega_I I_z + \omega_S S_z + \pi J_{IS} 2I_z S_z, \quad (2)$$

and

$$\begin{aligned} H_{\text{rf}}^{(\text{LF})}(\tau) = & \omega_1^I \{ I_x \cos[\omega_{\text{rf}}^I \tau + \phi_I(\tau)] + I_y \sin[\omega_{\text{rf}}^I \tau + \phi_I(\tau)] \} \\ & + \omega_1^S \{ S_x \cos[\omega_{\text{rf}}^S \tau + \phi_S(\tau)] \\ & + S_y \sin[\omega_{\text{rf}}^S \tau + \phi_S(\tau)] \}, \end{aligned} \quad (3)$$

where ω_k , with $k=I,S$, is the Larmor angular frequency of spin I or S , J_{IS} is the scalar-coupling constant, and ω_{rf}^k , ω_1^k , and ϕ_k , with $k=I,S$, are the carrier angular frequencies, nutation angular frequencies, and phases of the rf fields. In a doubly rotating frame (DRF) which precesses about the z axis at the two rf (angular) frequencies ω_{rf}^I for spin I and ω_{rf}^S for spin S , the Hamiltonian may be written as

$$H^{(\text{DRF})}(\tau) = H_0^{(\text{DRF})} + H_{\text{rf}}^{(\text{DRF})}[\phi_I(\tau), \phi_S(\tau)], \quad (4)$$

with

$$H_0^{(\text{DRF})} = \Omega_I I_z + \Omega_S S_z + \pi J_{IS} 2I_z S_z, \quad (5)$$

where $\Omega_k = \omega_k - \omega_{\text{rf}}^k$ ($k=I,S$) is the angular frequency offset and

$$\begin{aligned} H_{\text{rf}}^{(\text{DRF})}[\phi_I(\tau), \phi_S(\tau)] = & \omega_1^I \{ I_x \cos[\phi_I(\tau)] + I_y \sin[\phi_I(\tau)] \\ & + S_x \cos[\phi_S(\tau)] + S_y \sin[\phi_S(\tau)] \}, \end{aligned} \quad (6)$$

where we have assumed that the rf field components of the Hamiltonian have the same amplitude for spins I and S , $\omega_1^I = \omega_1^S = \omega_1$, i.e., that the Hartmann–Hahn condition is fulfilled, and that the phases $\phi_I(\tau)$ and $\phi_S(\tau)$ are constant over the duration of a single pulse, within a composite-pulse

sequence, for instance. Note that we refer to the terms ω_1^I and ω_1^S as the amplitudes of the rf field Hamiltonians and not the amplitudes of the rf magnetic fields B_1^I and B_1^S . We will assume that the rf fields for spins I and S act only on their corresponding nuclear species and that the rf amplitude ω_1 is large compared to both the angular frequency offsets Ω_I and Ω_S and the scalar-coupling constant J_{IS} .

Henceforth we shall drop the superscript (DRF) and always refer to the Hamiltonian in the form of Eq. (4).

The effects of coherent processes, i.e., scalar couplings, offsets, and inhomogeneous rf fields, during a periodic rf pulse sequence can be taken into account by AHT.^{30,31} The Hamiltonian in the interaction frame of the rf fields is

$$\tilde{H}(\tau) = \hat{U}_{\text{rf}}^\dagger(\tau) H_0 \hat{U}_{\text{rf}}(\tau), \quad (7)$$

with the propagator \hat{U}_{rf} , describing the evolution during the n th pulse of the sequence, defined as

$$\begin{aligned} \hat{U}_{\text{rf}}(\tau) = & \exp\{-iH_{\text{rf}}[\phi_{I,n}, \phi_{S,n}]\tau_n\} \\ & \times \hat{\mathbb{T}} \left\{ \prod_{j=1}^{(n-1)} \exp\{-iH_{\text{rf}}[\phi_{I,j}, \phi_{S,j}]\tau_j\} \right\}, \end{aligned} \quad (8)$$

where $\hat{\mathbb{T}}$ is the Dyson time-ordering operator, $\phi_{I,j}$ and $\phi_{S,j}$ are the phases of the j th pulse, and $\tau = \sum_{j=1}^n \tau_j$. Under the assumption that H_{rf} is a periodic function of time, with a period T , one may define an average Hamiltonian using the Magnus expansion as

$$\tilde{H}^{(\text{av})} = \tilde{H}^{(0)} + \tilde{H}^{(1)} + \tilde{H}^{(2)} + \dots, \quad (9)$$

where the various orders are

$$\tilde{H}^{(0)} = \frac{1}{T} \int_0^T d\tau \tilde{H}(\tau), \quad (10a)$$

$$\tilde{H}^{(1)} = \frac{1}{2iT} \int_0^T d\tau \int_0^\tau d\tau' [\tilde{H}(\tau), \tilde{H}(\tau')], \quad (10b)$$

$$\begin{aligned} \tilde{H}^{(2)} = & -\frac{1}{6T} \\ & \times \int_0^T d\tau \int_0^\tau d\tau' \int_0^{\tau'} d\tau'' \{ [\tilde{H}(\tau), [\tilde{H}(\tau'), \tilde{H}(\tau'')]] \\ & + [\tilde{H}(\tau'), [\tilde{H}(\tau'), \tilde{H}(\tau)]] \}, \end{aligned} \quad (10c)$$

...

A prerequisite of AHT is that the observation is stroboscopic, i.e., the observables of interest are sampled synchronously with the period T . The average effect of scalar couplings and offsets may be described by the transformation

$$\sigma(T) = \exp[-i\tilde{H}^{(\text{av})}T]\sigma(0)\exp[i\tilde{H}^{(\text{av})}T], \quad (11)$$

where $\sigma(0)$ and $\sigma(T)$ are the density operators of the spin system at the beginning and at the end of one repetition period of the pulse sequence, respectively.

B. Average Hamiltonian during an HDR MLEV-32 sequence

The new HDR MLEV-32 pulse sequence can be written as

$$\begin{aligned} & \bar{R}_a R_a R_a \bar{R}_a \bar{R}_a \bar{R}_a R_a R_a R_a \bar{R}_a \bar{R}_a R_a R_a R_a \bar{R}_a \bar{R}_a \\ & \bar{R}_b R_b R_b \bar{R}_b \bar{R}_b \bar{R}_b R_b R_b R_b \bar{R}_b \bar{R}_b R_b R_b R_b \bar{R}_b \bar{R}_b, \quad (12) \end{aligned}$$

where the overbars represent π phase shifts and where R_a and R_b represent composite pulses applied simultaneously to both spins I and S ,

$$R_a = \begin{Bmatrix} \beta_x^I & 2\beta_y^I & \beta_x^I \\ \beta_x^S & 2\beta_y^S & \beta_x^S \end{Bmatrix}, \quad R_b = \begin{Bmatrix} \beta_x^I & 2\beta_y^I & \beta_x^I \\ \beta_x^S & 2\beta_y^S & \beta_x^S \end{Bmatrix}, \quad (13)$$

where $\beta^I = \beta^S \approx \pi/2$. In the following we shall consider the ideal case $\beta^I = \beta^S = \pi/2$ unless mentioned otherwise. Deviations of β from $\pi/2$ will be treated as perturbations in Sec. III.

One may notice that Eqs. (12) and (13) actually define an MLEV-16 sequence \mathbb{K}_a based on the element R_a , followed by a second MLEV-16 sequence \mathbb{K}_b based on R_b . For spin I one has $\mathbb{K}_a^I = \mathbb{K}_b^I$, and the sequence thus turns out to be an MLEV-16 cycle applied twice. On the other hand, for spin S one has $\mathbb{K}_a^S = \mathbb{K}_b^S$, which gives a true MLEV-32 cycle. Simulations, discussed in Sec. IV, have shown that a real MLEV-32 cycle applied simultaneously to both spins does not work as well as the HDR sequence defined above.

Let us consider the first composite-pulse \bar{R}_a of the HDR MLEV-32 sequence. The corresponding rf propagator can be written as

$$\hat{U}_{\text{rf}}^{\bar{R}_a}(\tau) = \begin{cases} \exp[-iH_{\text{rf}}(\pi, \pi)\tau], & 0 \leq \tau < \tau_p, \\ \exp[-iH_{\text{rf}}(-\pi/2, \pi/2)\tau] \exp\left[-i\frac{H_{\text{rf}}(\pi, \pi)\pi}{\omega_1} \frac{\tau}{2}\right], & \tau_p \leq \tau < 3\tau_p, \\ \exp[-iH_{\text{rf}}(\pi, \pi)\tau] \exp\left[-i\frac{H_{\text{rf}}(-\pi/2, \pi/2)\pi}{\omega_1}\right] \exp\left[-i\frac{H_{\text{rf}}(\pi, \pi)\pi}{\omega_1} \frac{\tau}{2}\right], & 3\tau_p \leq \tau < 4\tau_p, \end{cases} \quad (14)$$

where $\tau_p = \pi/(2\omega_1)$ is the duration of an ideal $\pi/2$ pulse and where the three components correspond to three sequential pulses $\pi/2 - \pi - \pi/2$. The complete propagator up to the end of the first composite-pulse \bar{R}_a takes the form

$$\hat{U}_{\text{rf}}^{\bar{R}_a} \equiv \hat{U}_{\text{rf}}^{\bar{R}_a}(4\tau_p) = \exp\left[-i\frac{H_{\text{rf}}(\pi, \pi)\pi}{\omega_1} \frac{\pi}{2}\right] \exp\left[-i\frac{H_{\text{rf}}(-\pi/2, \pi/2)\pi}{\omega_1}\right] \exp\left[-i\frac{H_{\text{rf}}(\pi, \pi)\pi}{\omega_1} \frac{\pi}{2}\right], \quad (15)$$

and its matrix representation shows that $\hat{U}_{\text{rf}}^{\bar{R}_a} = 4I_y S_y$. By changing the phases ϕ_k ($k=I, S$) in Eqs. (14) and (15) according to the definition given in Eq. (13), one can define also the propagators $\hat{U}_{\text{rf}}^{R_a}(\tau)$, $\hat{U}_{\text{rf}}^{R_b}(\tau)$, and $\hat{U}_{\text{rf}}^{\bar{R}_b}(\tau)$, and verify by explicit matrix-algebra calculations that the following equalities hold for the propagators of each full composite pulse:

$$\hat{U}_{\text{rf}}^{R_a} \equiv \hat{U}_{\text{rf}}^{\bar{R}_a} = \hat{U}_{\text{rf}}^{R_a} = 4I_y S_y, \quad (16a)$$

$$\hat{U}_{\text{rf}}^{\bar{R}_b} = \hat{U}_{\text{rf}}^{R_b} = -4I_y S_y = -\hat{U}_{\text{rf}}^{R_b}, \quad (16b)$$

$$\hat{U}_{\text{rf}}^{\bar{R}_a} \hat{U}_{\text{rf}}^{R_a} = \mathcal{E}, \quad (16c)$$

where \mathcal{E} is the identity operator. Finally, by inserting the expressions of the rf propagators given by Eq. (14) into Eq. (7), the coherent Hamiltonian H_0 can be transformed into the rf interaction frame. During the first block of composite pulses ($\bar{R}_a R_a R_a \bar{R}_a$) of the HDR MLEV-32 sequence one has

$$\tilde{H}(\tau) = \begin{cases} \left(\hat{U}_{\text{rf}}^{\bar{R}_a}(\tau)\right)^\dagger H_0 \hat{U}_{\text{rf}}^{\bar{R}_a}(\tau), & 0 \leq \tau < 4\tau_p, \\ \left(\hat{U}_{\text{rf}}^{R_a}(\tau)\right)^\dagger \left(\hat{U}_{\text{rf}}^{\bar{R}_a}(\tau)\right)^\dagger H_0 \hat{U}_{\text{rf}}^{R_a}(\tau) \hat{U}_{\text{rf}}^{R_a}, & 4\tau_p \leq \tau < 8\tau_p, \\ \left(\hat{U}_{\text{rf}}^{R_a}(\tau)\right)^\dagger \left(\hat{U}_{\text{rf}}^{R_a}(\tau)\right)^\dagger \left(\hat{U}_{\text{rf}}^{\bar{R}_a}(\tau)\right)^\dagger H_0 \hat{U}_{\text{rf}}^{R_a}(\tau) \hat{U}_{\text{rf}}^{R_a} \hat{U}_{\text{rf}}^{\bar{R}_a} = \left(\hat{U}_{\text{rf}}^{\bar{R}_a}(\tau)\right)^\dagger H_0 \hat{U}_{\text{rf}}^{\bar{R}_a}(\tau), & 8\tau_p \leq \tau < 12\tau_p, \\ \left(\hat{U}_{\text{rf}}^{\bar{R}_a}(\tau)\right)^\dagger \left(\hat{U}_{\text{rf}}^{\bar{R}_a}(\tau)\right)^\dagger H_0 \hat{U}_{\text{rf}}^{\bar{R}_a}(\tau) \hat{U}_{\text{rf}}^{\bar{R}_a}, & 12\tau_p \leq \tau < 16\tau_p. \end{cases} \quad (17)$$

At the end of the full block one has $\tilde{H}(16\tau_p) = (\hat{U}_{\text{rf}}^R)^\dagger (\hat{U}_{\text{rf}}^R)^\dagger H_0 \hat{U}_{\text{rf}}^R \hat{U}_{\text{rf}}^R = H_0$, and therefore the Hamiltonian H_0 turns out to be in its original state. This property is true for any block of four composite pulses (MLEV-4). The procedure outlined above can be iterated for all eight blocks of composite pulses of the HDR MLEV-32 pulse sequence, and the zeroth-order average Hamiltonian [Eq. (10a)] can then be calculated as the sum of 96 integrals (one for each pulse of the sequence), with the period of the MLEV-32 sequence $T = 64\pi/\omega_1 = 128\tau_p$. The explicit calculations, based on straightforward matrix algebra, show that

$$\tilde{H}_{\text{MLEV}}^{(0)} = \frac{\pi J_{IS}}{4} 2I_z S_z. \quad (18)$$

The offsets Ω_I and Ω_S do not contribute to the zeroth-order term, which only depends on the J_{IS} coupling constant. The factor 1/4 in Eq. (18) corresponds to a scaling down of the scalar-coupling interaction produced by rotational averaging of the operators over the x , y , and z spatial orientations.

C. The zeroth-order effect

The effect of $\tilde{H}_{\text{MLEV}}^{(0)}$ on the density operator $\sigma(t)$ during the HDR MLEV-32 pulse sequence can be calculated according to Eq. (11) by replacing the general average Hamiltonian $\tilde{H}^{(\text{av})}$ with the zeroth-order term $\tilde{H}_{\text{MLEV}}^{(0)}$. The resulting equation shows that the dynamics of MQ coherences is not affected by $\tilde{H}_{\text{MLEV}}^{(0)}$ since the operator $2I_z S_z$ commutes with all MQC operators, $2I_x S_x$, $2I_x S_y$, $2I_y S_x$, and $2I_y S_y$, which are thus invariant after any integer number of complete HDR cycles.

It is interesting to compare the above results to a simplified HDR pulse sequence with the same phases for both the spins I and S , i.e., when R_a and R_b are replaced by the same composite pulses

$$R_c = \begin{Bmatrix} \beta_x^I & 2\beta_y^I & \beta_x^I \\ \beta_x^S & 2\beta_y^S & \beta_x^S \end{Bmatrix}, \quad (19)$$

with $\beta^I = \beta^S \approx \pi/2$. This sequence is equivalent to an MLEV-16 cycle applied simultaneously to both spins. The state of the system at the end of the HDR cycle may be described by solving the Liouville–von Neumann equation

$$\frac{d}{dt} \sigma(t) = -i[\tilde{H}^{(0)}, \sigma(t)], \quad (20)$$

which leads to

$$\frac{d}{dt} \begin{bmatrix} I_z \\ S_z \\ 2I_x S_y \\ 2I_y S_x \\ 2I_x S_x \\ 2I_y S_y \end{bmatrix} = \frac{\pi J_{IS}}{4} \begin{bmatrix} 0 & 0 & -2 & 1 & 0 & 0 \\ 0 & 0 & 1 & -2 & 0 & 0 \\ 2 & -1 & 0 & 0 & 0 & 0 \\ -1 & 2 & 0 & 0 & 0 & 0 \\ 0 & 0 & 0 & 0 & 0 & 0 \\ 0 & 0 & 0 & 0 & 0 & 0 \end{bmatrix} \begin{bmatrix} I_z \\ S_z \\ 2I_x S_y \\ 2I_y S_x \\ 2I_x S_x \\ 2I_y S_y \end{bmatrix}. \quad (21)$$

Clearly, this simplified sequence induces undesirable cross terms between the MQ and Zeeman subspaces.

D. Higher-order average Hamiltonians

We consider now the effects of higher-order terms in the expansion of Eq. (9). All odd-order average Hamiltonians vanish because of symmetry properties.³² As a consequence, the next higher-order term that may affect the dynamics of the system is $\tilde{H}^{(2)}$, defined in Eq. (10c). The (rather cumbersome) explicit calculations yield

$$\tilde{H}_{\text{MLEV}}^{(2)} = \frac{1}{\omega_1^2} \frac{J_{IS}}{48} [(20 - 7\pi)\Omega_I^2 - 20\pi\Omega_I\Omega_S + (20 - 7\pi)\Omega_S^2] 2I_z S_z. \quad (22)$$

The structure of this Hamiltonian closely resembles the zeroth-order term $\tilde{H}_{\text{MLEV}}^{(0)}$ of Eq. (18), thus extending the invariance of MQC operators to second-order effects. The amplitude of $\tilde{H}_{\text{MLEV}}^{(2)}$ defined in Eq. (22) becomes comparable to the amplitude of $\tilde{H}_{\text{MLEV}}^{(0)}$ when $|\Omega_I\Omega_S| \approx \omega_1^2$.

E. Average Hamiltonian during an HDR WALTZ-32 sequence

An alternative to the HDR MLEV-32 cycle treated in Secs. II B–II D is the HDR WALTZ-32 pulse sequence defined as

$$R_d \bar{R}_d \bar{R}_d R_d R_e \bar{R}_e \bar{R}_e R_e, \quad (23)$$

where R_d is

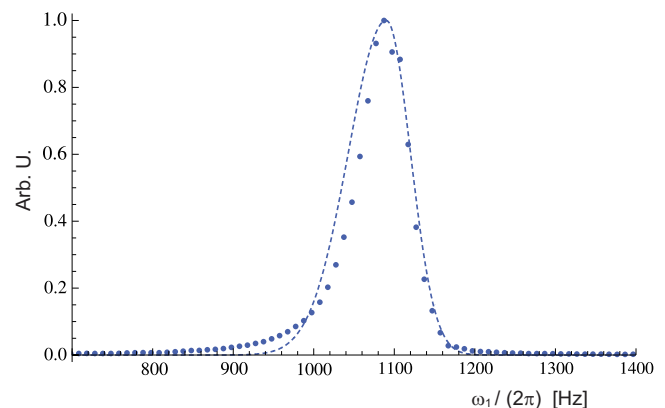


FIG. 1. (Color online) Distribution of the rf field ω_1 measured with a nutation experiment (filled circles) and fit of the experimental data obtained with two half-Gaussian functions of different widths (dashed line). More details are given in the text.

$$R_d = \begin{cases} 3\beta_{-x}^I & 4\beta_x^I & 2\beta_{-x}^I & 3\beta_x^I & \beta_{-x}^I & 2\beta_x^I & 4\beta_{-x}^I & 2\beta_x^I & 3\beta_{-x}^I \\ 3\beta_{-x}^S & 4\beta_x^S & 2\beta_{-x}^S & 3\beta_x^S & \beta_{-x}^S & 2\beta_x^S & 4\beta_{-x}^S & 2\beta_x^S & 3\beta_{-x}^S \end{cases}, \quad (24)$$

and R_e is

$$R_e = \begin{cases} 3\beta_{-x}^I & 4\beta_x^I & 2\beta_{-x}^I & 3\beta_x^I & \beta_{-x}^I & 2\beta_x^I & 4\beta_{-x}^I & 2\beta_x^I & 3\beta_{-x}^I \\ 3\beta_{-x}^S & 4\beta_x^S & 2\beta_{-x}^S & 3\beta_x^S & \beta_{-x}^S & 2\beta_x^S & 4\beta_{-x}^S & 2\beta_x^S & 3\beta_{-x}^S \end{cases}, \quad (25)$$

with β^I and β^S defined as in Sec. II B. The first block in Eq. (23) ($R_d \bar{R}_d \bar{R}_d R_d$) corresponds to a true WALTZ-16 sequence applied simultaneously to both spins, whereas during the second block ($R_e \bar{R}_e \bar{R}_e R_e$) the phases of the pulses applied to spin S are shifted by π . Simulations have shown that the efficiency of preservation of MQ coherences of this sequence is better than other alternatives, i.e., a true WALTZ-16 cycle applied twice to both spins simultaneously or a cycle in which, during the second block, the phases of the pulses applied to both spins I and S are shifted by π .

The procedure outlined in Sec. II B can also be applied to the HDR WALTZ-32 sequence. The calculations, based on simple matrix algebra, are rather cumbersome and not of

prime interest and therefore not shown explicitly here. The two nonzero lowest-order average Hamiltonians turn out to be

$$\tilde{H}_{\text{WALTZ}}^{(0)} = \frac{\pi J_{IS}}{2} 2I_z S_z, \quad (26)$$

and

$$\begin{aligned} \tilde{H}_{\text{WALTZ}}^{(2)} = & -\frac{1}{\omega_1^2} \frac{J_{IS}}{576} [21J_{IS}^2 \pi^3 \\ & + 4(10 + 49\pi)(\Omega_I^2 + \Omega_S^2)] 2I_z S_z. \end{aligned} \quad (27)$$

All orders of the average Hamiltonians that were computed commute with the MQ operators of interest so that the effects

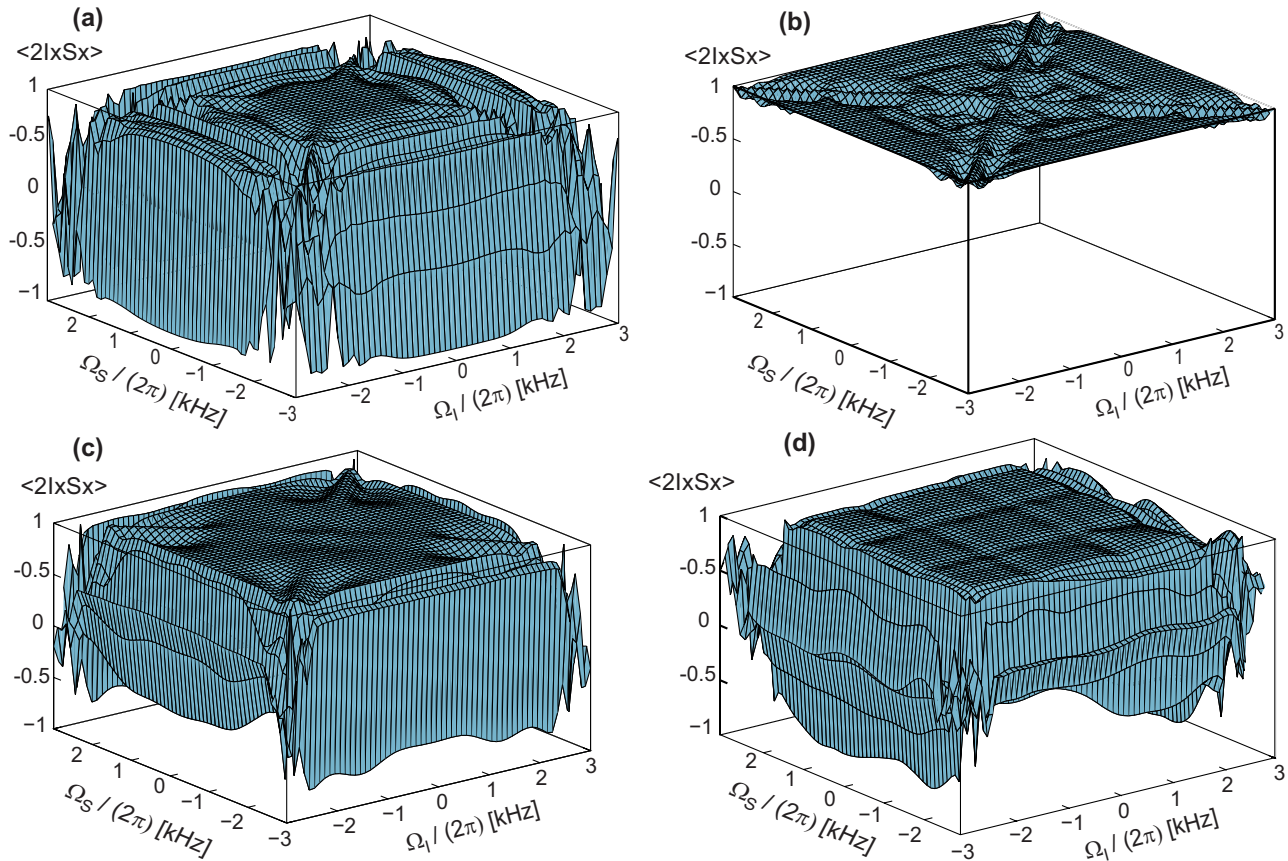


FIG. 2. (Color online) Simulations of the expectation value of the coherence $2I_x S_x$ as a function of the offsets Ω_I and Ω_S of spins I and S after different HDR pulse sequences based on (a) DIPSI, (b) GARP, (c) WALTZ-32, and (d) MLEV-32 blocks with a scalar-coupling constant $J_{IS}=90$ Hz and an rf field amplitude $\omega_1/(2\pi)=2$ kHz. We have set the initial density operator $\sigma(0)=2I_x S_x$ and the durations of the sequences were (a) $T=28.8$ ms, (b) 31.2 ms, (c) 48 ms, and (d) 32 ms. These durations correspond to 1 cycle of the DIPSI and GARP schemes and 2 cycles of the HDR WALTZ-32 sequence given in Eq. (23) and of the HDR MLEV-32 sequence given in Eq. (12).

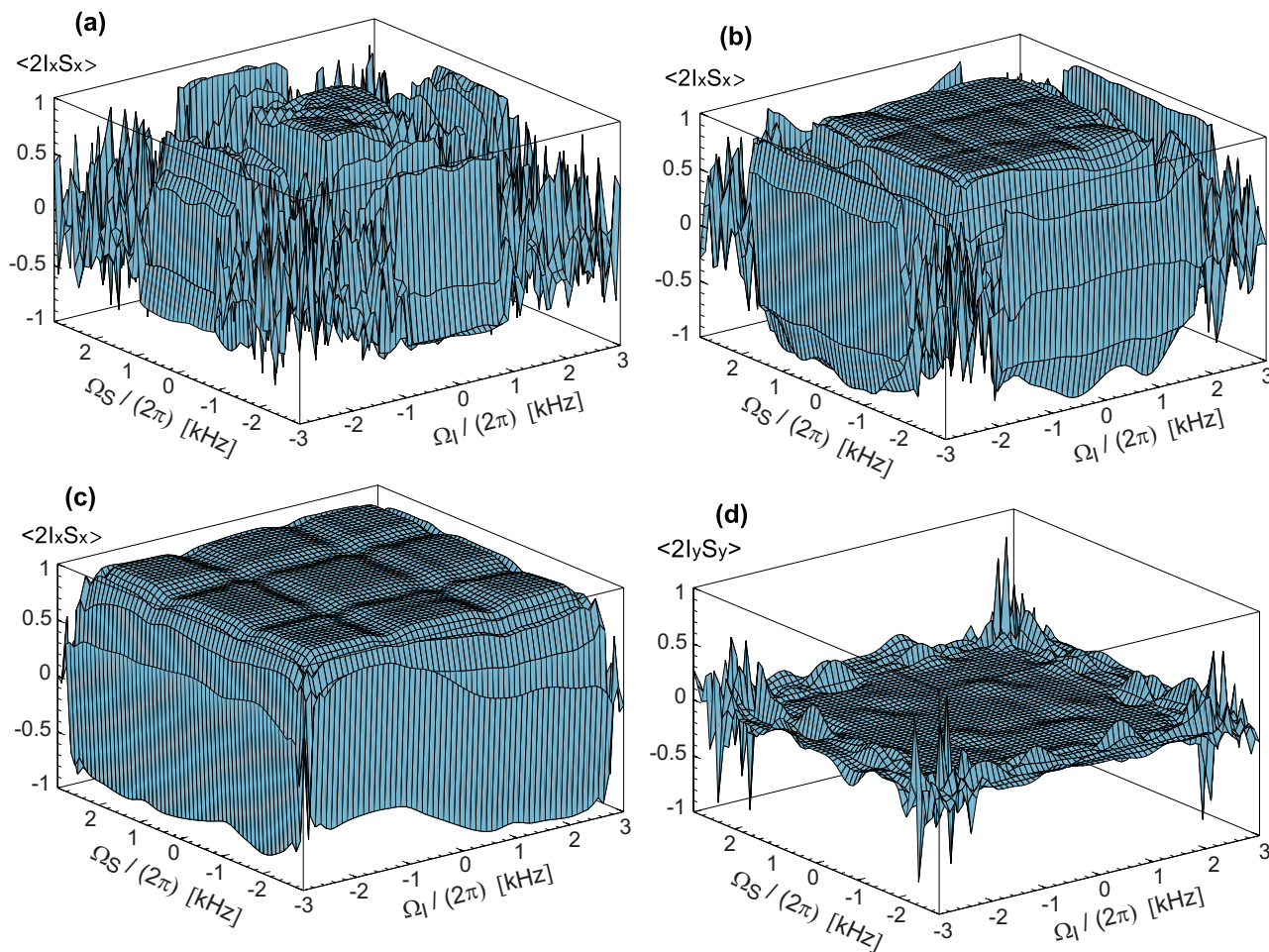


FIG. 3. (Color online) Simulations of the expectation values of the heteronuclear MQ coherences $2I_x S_x$ [(a)–(c)] and $2I_y S_y$ (d) as a function of the offsets Ω_k ($k=I,S$) of spins I and S after the HDR MLEV-32 sequence assuming a scalar-coupling constant $J_{IS}=90$ Hz. The rf amplitudes for both spins are (a) $\omega_1/(2\pi)=0.8$ kHz with a single HDR MLEV-32 block, (b) $\omega_1/(2\pi)=1.6$ kHz with two HDR MLEV-32 blocks, (c) $\omega_1/(2\pi)=2.4$ kHz with three blocks, and (d) $\omega_1/(2\pi)=2.0$ kHz with two blocks as in Fig. 2(d). The duration of the HDR sequences (a)–(c) was $T=40$ ms, while in (d) $T=32$ ms. The initial density operator was $\sigma(0)=2I_x S_x$. The $\langle 2I_y S_y \rangle$ profile (d) shows that during the rf sequence coherent leakage from the initial operator $2I_x S_x$ to $2I_y S_y$ is small for offsets as large as $\Omega_k \approx \pm \omega_1$.

of offsets and scalar couplings much smaller than the rf amplitudes can be neglected. Similar to the average Hamiltonian of the HDR MLEV-32 sequence, the zeroth-order term does not depend on the offsets Ω_I and Ω_S but only on the scalar-coupling constant J_{IS} . One may also notice that $\tilde{H}_{\text{WALTZ}}^{(0)}=2\tilde{H}_{\text{MLEV}}^{(0)}$. Intuitively, this last property makes the WALTZ-32 sequence less robust with respect to scalar-coupling effects than the MLEV-32 sequence. This conclusion is indeed supported by numerical simulations.

III. INHOMOGENEOUS rf FIELDS

A. Experiment

We have measured the distribution of the rf field $\omega_1/(2\pi)$ with a nutation experiment on the nitrogen-15 channel of a TCI cryoprobe on a Bruker Avance 500 spectrometer. The sample consisted of 250 μl of a solution of ^{15}N labeled and selectively deuterated *t*Boc-glycine in perdeuterated dimethyl sulfoxide (DMSO) in a Shigemi tube. The result of the experiment is shown in Fig. 1 (filled circles).³³ In order to have a reliable model for numerical simulations

(presented in Sec. IV) we have fitted the experimental data with two half-Gaussian functions of different widths,

$$f_{\text{fit}}[\omega_1/(2\pi)] = \begin{cases} \exp\left[\frac{1}{(2\pi)^2} \frac{(\omega_1 - \omega_c)^2}{2\sigma_1^2}\right], & \omega_1 < \omega_c, \\ \exp\left[\frac{1}{(2\pi)^2} \frac{(\omega_1 - \omega_c)^2}{2\sigma_2^2}\right], & \omega_1 \geq \omega_c. \end{cases} \quad (28)$$

In Fig. 1 (dashed line) we have used $\omega_c/(2\pi)=1090$ Hz, $\sigma_1=47$ Hz, and $\sigma_2=30$ Hz. The full width at half maximum (FWHM) of the fitting function thus turns out to be $\approx 10\%$ of the carrier frequency. Henceforth, we will assume this distribution model for both the spins, independent of the carrier frequency.

B. Average Hamiltonian theory

The AHT outlined in Sec. II can be applied to treat the effects of inhomogeneities of the rf fields. During a complete HDR pulse sequence we shall assume a perfectly calibrated

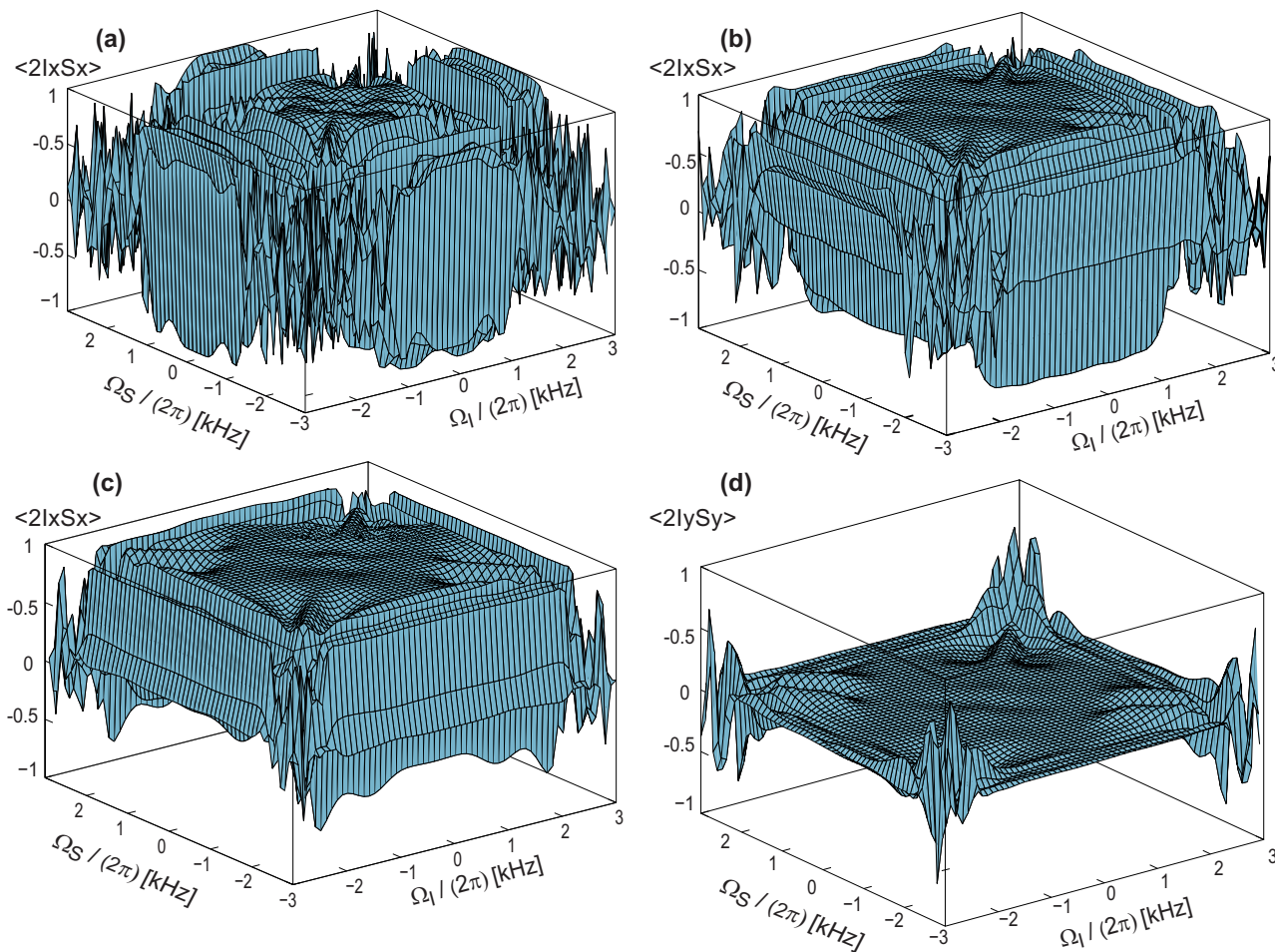


FIG. 4. (Color online) Simulations of the expectation values of the heteronuclear MQ coherences $2I_x S_x$ [(a)–(c)] and $2I_y S_y$ (d) as a function of the offsets Ω_k ($k=I, S$) of spins I and S after the HDR WALTZ-32 sequence assuming a scalar-coupling constant $J_{IS}=90$ Hz. The rf amplitudes for both spins are (a) $\omega_1/(2\pi)=1$ kHz with a single HDR WALTZ-32 block, (b) $\omega_1/(2\pi)=1.4$ kHz also with a single HDR WALTZ-32 block, (c) $\omega_1/(2\pi)=1.8$ kHz with two blocks, and (d) $\omega_1/(2\pi)=2.0$ kHz with two blocks as in Fig. 2(c). The durations of the HDR sequences were $T=48$ ms (a), $T=34.28$ ms (b), $T=53.32$ ms (c), and $T=48$ ms (d). The initial density operator was $\sigma(0)=2I_x S_x$. The $\langle 2I_y S_y \rangle$ profile (d) shows that coherent leakage from $2I_x S_x$ to $2I_y S_y$ is small for offsets as large as $\Omega_k \approx \pm \omega_1$.

rf interaction, described by the ideal Hamiltonian H_{rf} of Eq. (6), plus a perturbation that we may write in the form

$$H_{\epsilon}[\phi_I(\tau), \phi_S(\tau)] = \omega_{\epsilon}^I \{ I_x \cos[\phi_I(\tau)] + I_y \sin[\phi_I(\tau)] \} + \omega_{\epsilon}^S \{ S_x \cos[\phi_S(\tau)] + S_y \sin[\phi_S(\tau)] \}, \quad (29)$$

with $\omega_{\epsilon}^k = (\beta^k - \pi/2)/\tau_p$, where β^k is the actual nutation angle and $k=I, S$. The evolution of the system under the effect of the (inhomogeneous) rf fields is thus governed by the Hamiltonian

$$H_{\text{rf}}^{(\text{inh})} = H_{\text{rf}}[\phi_I(\tau), \phi_S(\tau)] + H_{\epsilon}[\phi_I(\tau), \phi_S(\tau)], \quad (30)$$

and the procedure described in Sec. II B can be applied by substituting H_0 by H_{ϵ} . One can thus transform H_{ϵ} into the rf interaction frame [see Eq. (17)] and calculate explicitly the zeroth-, first-, and second-order average Hamiltonians. The calculations show that all the contributions to the average Hamiltonian up to second order vanish. One may thus expect that perturbations of the form H_{ϵ} , i.e., imperfections of the rf fields, would not affect the dynamics of the spin system under the HDR MLEV-32 sequence. The first three orders of

the average Hamiltonian were also calculated for the HDR WALTZ-32 sequence, with identical results. The low sensitivity of MQC operators to the effect of small rf field inhomogeneities has been confirmed by simulations, as shown in Sec. IV.

IV. SIMULATIONS

The AHT results discussed in Sec. II are valid in the limits $\pi|J_{IS}| \ll |\omega_1|$ and $|\Omega_I|, |\Omega_S| \ll |\omega_1|$, i.e., close to resonance. Under these conditions one can treat the evolution under scalar couplings and offsets as perturbations in the interaction frame. In order to estimate the effects of a rather large scalar-coupling constant over a wide range of offsets and rf amplitudes we have carried out numerical simulations.

The main purpose of our sequence is to preserve all MQ coherences over a range of offsets that is as large as possible. In the ideal case, we should be able to cover the resonance frequencies of all residues of a protein in a single experiment. Therefore, we have simulated the behavior of MQ coherences under the effect of several HDR sequences, based on well-known methods such as WALTZ-16,²⁹ WALTZ-32, GARP,³⁴ DIPSI,³⁵ XY-32,³⁶ MLEV-16, and MLEV-32.^{25–28}

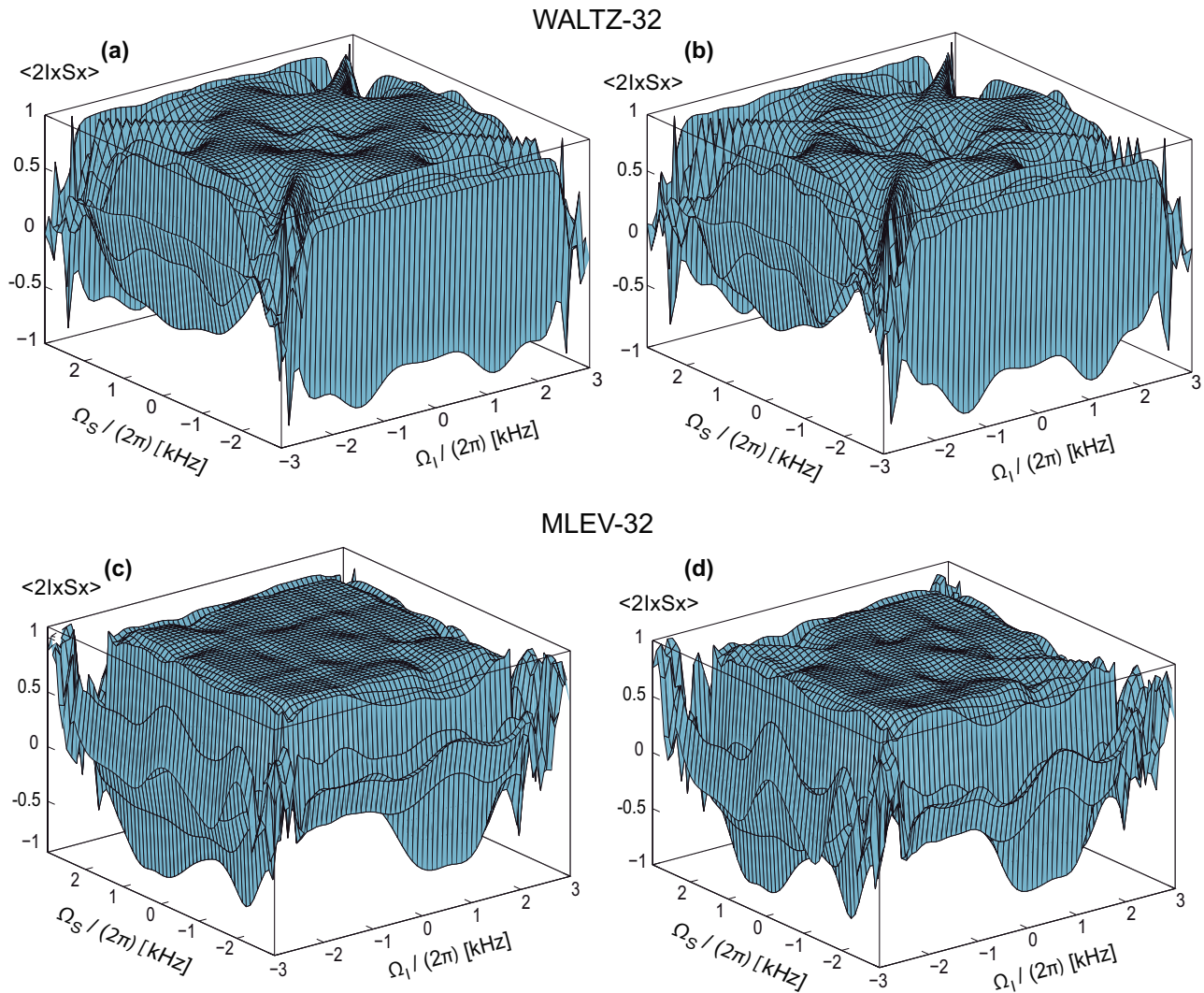


FIG. 5. (Color online) Simulations of the expectation value $\langle 2I_x S_x \rangle$ as a function of the offsets Ω_k ($k=I, S$) of spins I and S after the HDR WALTZ-32 sequence [(a) and (b)] and after the HDR MLEV-32 sequence [(c) and (d)]. We have assumed scalar-coupling constants [(a) and (c)] $J_{IS}=150$ Hz and [(b) and (d)] $J_{IS}=200$ Hz. The rf amplitude for both spins was $\omega_1/(2\pi)=2$ kHz with two blocks of both the HDR WALTZ-32 and HDR MLEV-32 schemes. The durations of the HDR sequences were $T=48$ ms [(a) and (b)] and $T=32$ ms [(c) and (d)]. The initial density operator was $\sigma(0)=2I_x S_x$. These profiles should be compared to the profiles of Fig. 2(c) (HDR WALTZ-32) and Fig. 2(d) (HDR MLEV-32) obtained with $J_{IS}=90$ Hz.

Results for some of these sequences are shown in Fig. 2. We have tried different approaches. For instance, the sequences based on π phase shift of all pulses applied to spin S during the second half of the cycle turned out to be always better than sequences applied without any phase shift. The best performance was obtained with the HDR WALTZ-32 [Fig. 2(c)] and HDR MLEV-32 [Fig. 2(d)] pulse sequences. In Figs. 3 and 4 we plot the simulated profiles of the operators $\langle 2I_x S_x \rangle$ and $\langle 2I_y S_y \rangle$ for different rf amplitudes as a function of the offsets Ω_k , with $k=I, S$, after the HDR MLEV-32 (Fig. 3) and WALTZ-32 (Fig. 4) sequences. We have set the initial density operator $\sigma(0)=2I_x S_x$ and assumed $J_{IS}=90$ Hz. Identical results were obtained when starting with $2I_y S_y$. The profiles shown in Figs. 3 and 4 are characterized by a plateau which shows the efficiency of the pulse sequence in preserving MQ coherences over a wide range of offsets. The edges of this plateau correspond to values of the offsets Ω_I and Ω_S comparable to the rf amplitude ($\Omega_k \approx \pm \omega_1$). One can safely assume that over such a range of offsets the evolution of the system is not affected by scalar couplings and that

Hartmann–Hahn cross-polarization does not affect the dynamics of MQ coherences. Moreover, we have carried out simulations with a range of scalar-coupling constants J_{IS} from 50 to 200 Hz. In Fig. 5 we show the offset profiles obtained with HDR WALTZ-32 and HDR MLEV-32 sequences with $J_{IS}=150$ Hz [(a) and (c)] and $J_{IS}=200$ Hz [(b) and (d)]. We observed significant changes in the profiles obtained with the HDR MLEV-32 sequence only close to the limit $J_{IS} \approx 200$ Hz, whereas we observed a general deterioration of the performance of the WALTZ-32 sequence for scalar-coupling constants larger than about 120 Hz. The higher sensitivity to large scalar-coupling interactions of the HDR WALTZ-32 sequence compared to the HDR MLEV-32 scheme may be linked intuitively to the larger residual scalar coupling in the average Hamiltonian [see Eqs. (18) and (26)].

The effects of rf field inhomogeneities have been included in the simulations by considering the asymmetric distribution of rf amplitudes given in Eq. (28), sampled at 17 amplitudes ranging from $0.9\omega_1$ to $1.1\omega_1$. The parameters

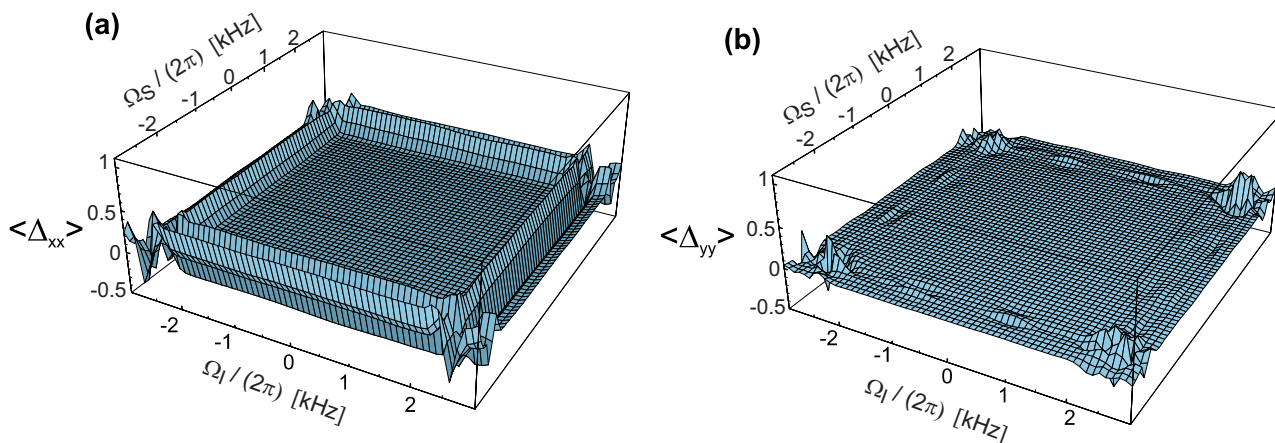


FIG. 6. (Color online) Simulated differential expectation values $\langle \Delta_{xx} \rangle = \langle 2I_x S_x \rangle_{\text{inh}} - \langle 2I_x S_x \rangle_{\text{hom}}$ (a) and $\langle \Delta_{yy} \rangle = \langle 2I_y S_y \rangle_{\text{inh}} - \langle 2I_y S_y \rangle_{\text{hom}}$ (b) of the MQ operators $2I_x S_x$ and $2I_y S_y$, respectively, as a function of the offsets Ω_k ($k=I, S$) of spins I and S after 2 cycles of the HDR MLEV-32 scheme, assuming a scalar-coupling constant $J_{IS}=90$ Hz, an rf amplitude $\omega_1/(2\pi)=2$ kHz, and an initial density operator $\sigma(0)=2I_x S_x$. The duration of the sequence was $T=32$ ms. These profiles show the differences of the profiles of $\langle 2I_x S_x \rangle$ (a) and $\langle 2I_y S_y \rangle$ (b) obtained with and without rf inhomogeneities.

σ_1 and σ_2 were chosen to produce a FWHM of $\approx 10\%$ of the carrier frequency. In the simulations we have assumed the same rf amplitude distribution for both spins, i.e., $\omega_1^I(\vec{r}) = \omega_1^S(\vec{r})$. The offset profiles simulated with correlated or uncorrelated rf inhomogeneities did not show any remarkable

differences compared to profiles obtained for ideal rf fields, at least in the regions where the MQ coherences can be preserved efficiently. In Fig. 6(a) we show the differential offset profile $\langle \Delta_{xx} \rangle = \langle 2I_x S_x \rangle_{\text{inh}} - \langle 2I_x S_x \rangle_{\text{hom}}$, i.e., the difference between the simulated profiles obtained with and without rf

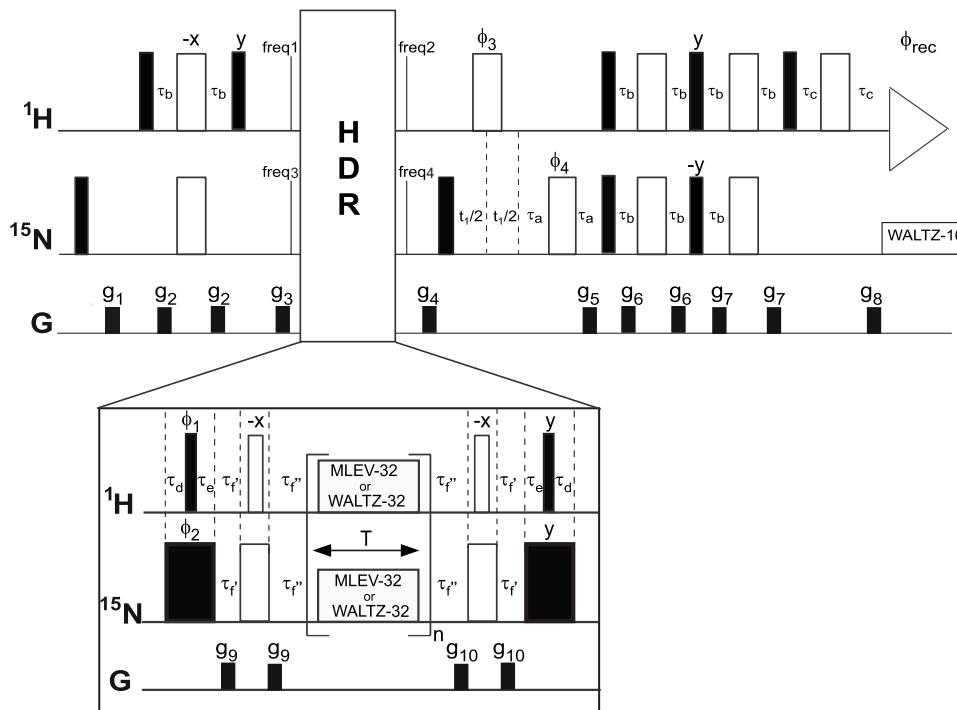


FIG. 7. Pulse sequence used to preserve the MQ coherence $H_x N_x$ of the N-H pair in deuterated ¹Boc-glycine. Filled and open rectangles represent $\pi/2$ and π pulses, respectively. The widths of the rectangles are not proportional to the actual durations of the rf pulses. All pulses are applied along the x -axes unless indicated otherwise. The proton carrier frequency is switched to the desired offset before the HDR block (freq1) and then switched back (freq2) to the center of the spectrum (3.5 ppm). The carrier frequency of the nitrogen-15 channel is switched to the desired frequency before the HDR block (freq3) and switched back to its initial value (freq4), 78.5 ppm, right after the HDR block. The delays are $\tau_{id} = t_{\pi/2}(^{15}\text{N}) - t_{\pi/2}(^1\text{H}) - \tau_e$, $\tau_e = [t_{\pi/2}(^{15}\text{N}) - t_{\pi/2}(^1\text{H})] \times 0.637$, $\tau_{f'} = 652 \mu\text{s}$, and $\tau_{f''} = 650 \mu\text{s} + t_{\pi/2}(^{15}\text{N}) \times 0.637$ with durations of strong $\pi/2$ pulses $t_{\pi/2}(^{15}\text{N}) = 35 \mu\text{s}$ and $t_{\pi/2}(^1\text{H}) = 6.62 \mu\text{s}$. These delays are inserted to compensate for chemical shift evolutions during the $\pi/2$ pulses on the proton and nitrogen channels. The echo pulses before the HDR blocks are needed to provide time to change the power levels from high amplitude to attenuated values for HDR pulses. The other delays are $\tau_a = 1.2$ ms, $\tau_b = 1/(4J_{\text{HN}})$, and $\tau_c = 1.157$ ms. The WALTZ-16 decoupling scheme at the end is applied using a low-amplitude rf field of 0.5 kHz. The duration of the acquisition is 500 ms. The gradients are $g_{1x} = 6.5$ G/cm, $g_{2y} = 8.5$ G/cm, $g_{3z} = 13.5$ G/cm, $g_{4z} = 15$ G/cm, $g_{5z} = 40$ G/cm, $g_{6x} = -9.5$ G/cm, $g_{7y} = 10.5$ G/cm, $g_{8z} = 4.05$ G/cm, $g_{9x} = 4.5$ G/cm, $g_{9y} = 5.5$ G/cm, $g_{10x} = 7.5$ G/cm, and $g_{10y} = 8.5$ G/cm. The phase cycling is $\phi_1 = (y)_4, (-y)_4$; $\phi_2 = (y, -y)$; $\phi_3 = (x, -x)$; $\phi_4 = (x)_2, (y)_2, (-x)_2, (-y)_2$; and $\phi_{\text{rec}} = (x, -x, -x, x)_2, (-x, x, x, -x)_2$.

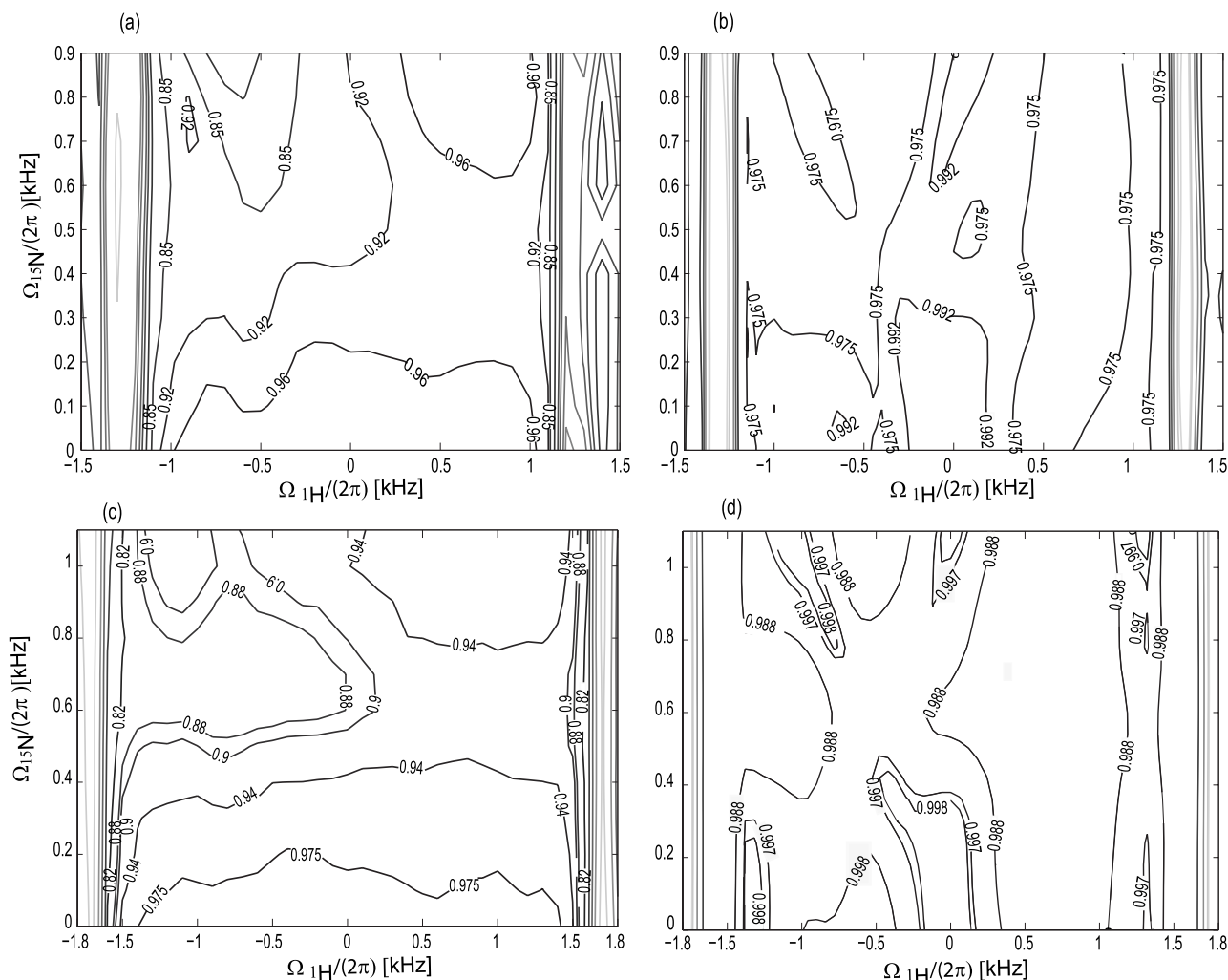


FIG. 8. [(a) and (c)] Experimental profiles of the expectation value $\langle 2I_x S_x \rangle$ after a single HDR MLEV-32 block for the ^{15}N - ^1H pair in $^1\text{Boc-glycine}$ (^{15}N , $^2\text{H}^\alpha$) as a function of the offsets of ^{15}N and ^1H obtained with rf amplitudes $\omega_1/(2\pi)$ of 1 kHz (a) and 1.4 kHz (c). The durations of the sequences were $T = 32$ ms (a) and $T = 23$ ms (c). [(b) and (d)] Corresponding simulations. The contour levels are expressed as percentage of the on-resonance peak intensity.

inhomogeneities after a HDR MLEV-32 sequence. In Fig. 6(b) we also show a similar differential profile $\langle \Delta_{yy} \rangle = \langle 2I_y S_y \rangle_{\text{inh}} - \langle 2I_y S_y \rangle_{\text{hom}}$, obtained after a HDR MLEV-32 sequence. Identical results were obtained for the HDR WALTZ-32 sequence (data not shown here). In both cases we have assumed a distribution of rf amplitudes with a maximum value for $\omega_1/(2\pi)$ of 2 kHz, a coupling constant $J_{IS} = 90$ Hz, and an initial density operator $\sigma(0) = 2I_x S_x$. These results did not change significantly by varying ω_1 and J_{IS} or by setting the initial state to $\sigma(0) = 2I_y S_y$.

V. METHODS

All symbolic calculations were carried out with the support of MATHEMATICA (Version 6.0) and all numerical calculations were performed under MATLAB R2007B (Version 7.5). The experimental characterization of the offset profiles was carried out for the ^{15}N - ^1H pair in selectively deuterated $^1\text{Boc-glycine}$, $(\text{CH}_3)_3\text{COCO-NHCD}_2\text{CO}_2\text{H}$ (^{15}N , $^2\text{H}^\alpha$), in DMSO. Deuteration is necessary to prevent dipolar cross-relaxation as well as cross-polarization effects between the H^ν and the two scalar-coupled H^α nuclei. All data were collected in a static magnetic field $B = 11.7$ T (500 MHz) on a

Bruker Avance 500 spectrometer equipped with a TCI cryoprobe. The full pulse sequence used in the experiments is shown in Fig. 7. In Figs. 8(a) and 8(c) we show the experimental profiles of the observable $\langle 2I_x S_x \rangle$ for the isolated ^{15}N - ^1H pair in $^1\text{Boc-glycine}$ with rf field amplitudes $\omega_1/(2\pi) = 1$ kHz (a) and 1.4 kHz (c), after the HDR MLEV-32 sequence. The durations of the HDR MLEV-32 sequences were $T = 32$ ms (a) and $T = 23$ ms (c). In both cases the block of Eq. (12) was repeated only once. The corresponding simulated contour plots obtained with the HDR sequence of Fig. 7 are shown in Figs. 8(b) and 8(d). In Figs. 9(a) and 9(c) we show the experimental profiles obtained with the HDR WALTZ-32 sequence, with rf field amplitudes $\omega_1/(2\pi) = 1.0$ kHz (a) and 1.6 kHz (c). The durations of the HDR WALTZ-32 sequences were $T = 48$ ms (a) and $T = 30$ ms (c), corresponding to one block of Eq. (23). In Figs. 9(b) and 9(d) we show the corresponding simulated contour plots. The simulations of Figs. 8 and 9 differ from those shown in Figs. 2-4 since in the former all pulses and delays shown in the "HDR" insert of Fig. 7 were simulated, whereas in the latter only the HDR cycle was considered.

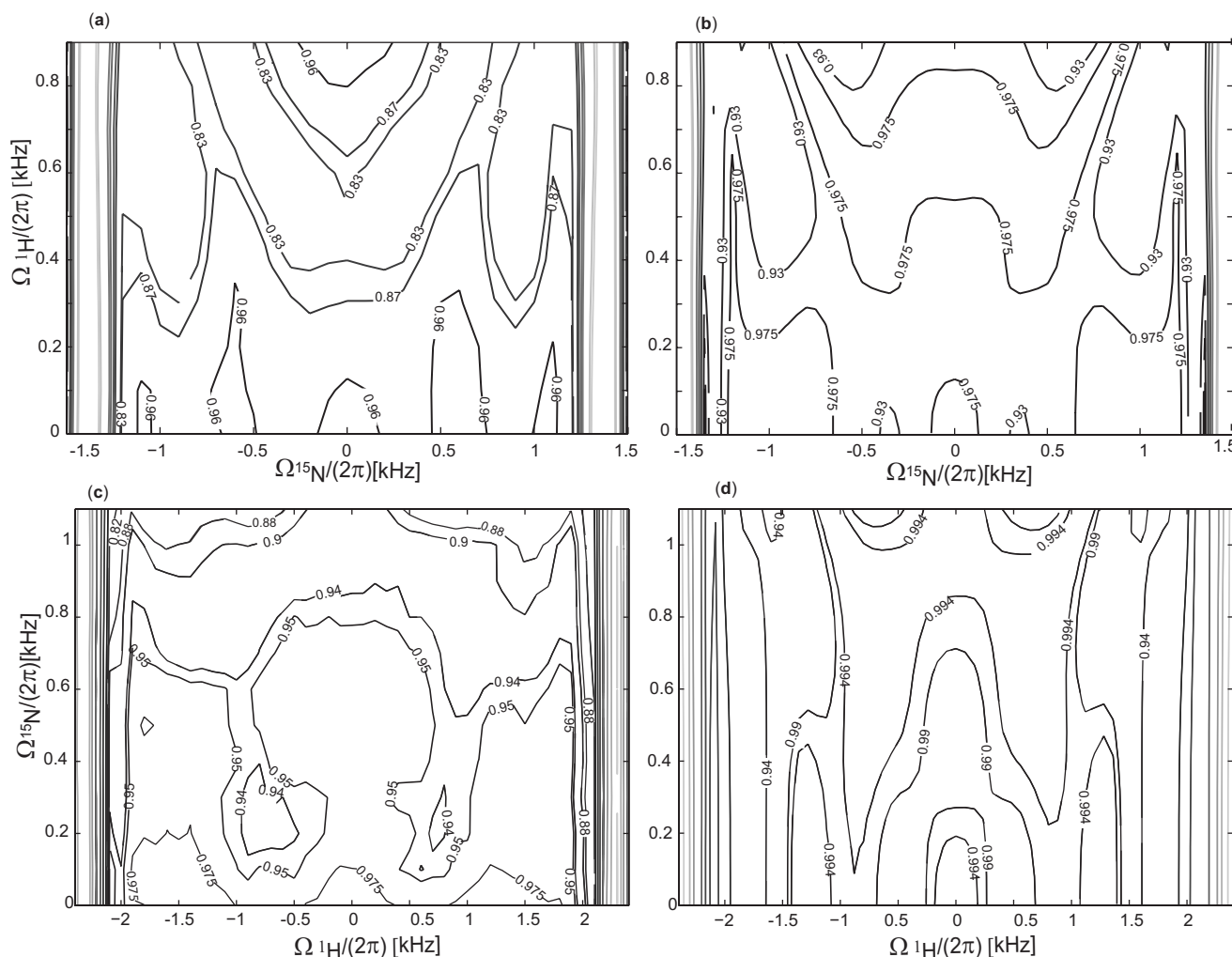


FIG. 9. [(a) and (c)] Experimental profiles of the expectation value $\langle 2I_x S_x \rangle$ after a single HDR WALTZ-32 block for the $^{15}\text{N}-^1\text{H}$ pair in Boc-glycine (^{15}N , $^2\text{H}^+$) as a function of the offsets of ^{15}N and ^1H channels obtained with rf amplitudes $\omega_1/(2\pi) = 1.6$ kHz (a) and 1.0 kHz (c). The durations of the sequences were $T = 30$ ms (a) and $T = 48$ ms (c). [(b) and (d)] Corresponding simulations. The contour levels are expressed as percentage of the on-resonance peak intensity.

VI. DISCUSSION

We have presented a new HDR method based on MLEV-32 and WALTZ-32 sequences applied simultaneously to spins I and S and we have developed a theoretical framework to treat the effects of coherent processes. The requirements for the effective preservation of multiple-quantum coherences are rather challenging, particularly when the objective is to determine small cross-relaxation rates between multiple-quantum operators. The ability to measure cross-relaxation rates between the MQ operators $2I_x S_x$ and $2I_y S_y$ presupposes the suppression of coherent pathways for their interconversion. The separation of coherent evolution and relaxation effects is difficult unless the MQ coherences are effectively forced to remain stationary under all coherent processes. On the other hand, since cross-relaxation pathways have to be retained, it is necessary to keep the evolution on both spins as synchronous as possible. Thus, the rf field amplitudes have to match the Hartmann-Hahn condition. This increases the risk of artifacts arising from undesirable cross-polarization.

All orders of the average Hamiltonian that were com-

puted commute with the operators under investigation (i.e., $2I_x S_x$ and $2I_y S_y$) so that effects of offsets, scalar couplings, and rf inhomogeneity can be neglected as long as they are small, i.e., when $\pi|J_{IS}| \ll |\omega_1|$ and $|\Omega_I|, |\Omega_S| \ll |\omega_1|$. Moreover, both simulations and experiments show that the offset profiles are reasonably flat for offsets as large as the rf amplitude. The effects of scalar couplings are limited if rf amplitudes are more than ten times larger than the scalar-coupling constant with the HDR MLEV-32 scheme (see Figs. 3–5). This means that the lowest rf amplitude for $^1\text{H}-^{13}\text{C}$ pairs would be of the order of 1.5 kHz. On the other hand, the deterioration of the preservation profiles for the HDR WALTZ-32 scheme [Figs. 5(a) and 5(b)] with large scalar-coupling constants restricts its use to systems with scalar-coupling constants smaller than ≈ 120 Hz for rf amplitudes of 2 kHz. As shown in Figs. 3(d) and 4(d) the coherent leakage between the operators $2I_x S_x$ and $2I_y S_y$ is effectively quenched on resonance and strongly inhibited off resonance. We have estimated the leakage level to be less than 1% for the HDR WALTZ-32 and less than 3% for the HDR MLEV-32 when $|\Omega_I|, |\Omega_S| \leq |\omega_1|/2$. The leakage increases to

about 7 % and 10% for the HDR WALTZ-32 and MLEV-32 sequences, respectively, when $|\Omega_I|, |\Omega_S| \approx |\omega_1|$. One should be aware that this leakage will limit the accuracy of cross-relaxation rates measured with these schemes when used significantly off resonance ($|\Omega_I|, |\Omega_S| > |\omega_1|/2$).

The comparison with various pulse sequences typically employed for decoupling,^{34,35} homonuclear isotropic mixing,³⁵ or isotropic spin locking,³⁶ is insightful. The sequence HDR XY-32 exhibits large variations in the observable of interest, even very close to resonance, suggesting that this multiple-refocusing sequence cannot be used for our purposes. Figure 2 shows that although two GARP sequences simultaneously applied to both nuclei provide a reasonably effective preservation of all MQ coherences over a broad range of offsets, small variations in the observable terms close to resonance make this scheme unreliable. On the other hand, DIPSI shows a very flat profile near resonance. However, the behavior further from resonance is not as good as for the HDR MLEV-32 and HDR WALTZ-32 schemes. The latter sequences seem to provide the best compromise between a nearly ideal flat offset profile close to resonance and a reasonably flat profile further from resonance. The periodic minima observed in the offset profiles of the HDR MLEV-32 scheme, shown in Figs. 3(b) and 3(c), may be due to recoupling conditions that are fulfilled for certain values of the offsets Ω_I and Ω_S and of the scalar-coupling constant J_{IS} . This pattern of local minima is altered for larger values of J_{IS} , as shown in Figs. 5(c) and 5(d). The offset profiles obtained with the HDR WALTZ-32 scheme do not exhibit an analogous periodic pattern of local minima [see Figs. 4(b) and 4(c)], and a continuous deterioration of the profiles was observed for increasing values of J_{IS} [Figs. 5(a) and 5(b)]. The tolerance to distributions of rf fields encountered in typical high-resolution probes, as illustrated in Fig. 6, shows that these sequences can be used with common equipment. The HDR MLEV-32 and WALTZ-32 sequences should also be fairly insensitive to small miscalibrations of the rf amplitudes.

It may be interesting to compare the expressions of the second-order average Hamiltonians given in Eqs. (22) and (27) with the offset profiles shown in Sec. IV. For MLEV-32, $\tilde{H}_{\text{MLEV}}^{(2)}$ depends on the relative sign of the offsets Ω_I and Ω_S as it is dominated by the term $\Omega_I\Omega_S$, while for WALTZ-32, $\tilde{H}_{\text{WALTZ}}^{(2)}$ is dominated by $(\Omega_I^2 + \Omega_S^2)$. Interestingly, the simulated offset profiles of the HDR WALTZ-32 sequence are symmetric, whereas the offset profiles of the HDR MLEV-32 sequence exhibit different behaviors along the diagonal ($\Omega_I = \Omega_S$) and the antidiagonal ($\Omega_I = -\Omega_S$). Similarities between the expressions of the second-order terms in the average Hamiltonians and the symmetry properties of the offset profiles are intuitively satisfying. They suggest that higher-order terms in the average Hamiltonian exhibit a structure similar to second-order terms.

The agreement between experiments and simulations shown in Fig. 8 (HDR MLEV-32) and in Fig. 9 (HDR WALTZ-32) is reasonably good. The patterns of the deviations from an ideal preservation of all MQ coherences are comparable but the amplitudes of such deviations are signifi-

cantly larger in experiments than in simulations. For instance, the small “valleys” that can be seen on the plateau in Figs. 3(b) and 8(d) [or Figs. 4(b), 9(b), and 9(d)] are also found in Fig. 8(c) [or Figs. 9(a) and 9(c)], where they are both deeper and wider. These differences may arise because of coherent processes that have been neglected, imperfections of the hardware, or relaxation effects. The treatment of the latter is beyond the scope of this paper and will be discussed elsewhere. The faster decay of multiple-quantum coherences off resonance significantly affects the measurement of autorelaxation rates. On the other hand, the accuracy of cross-relaxation rates should be preserved, in particular, if symmetrical reconversion is employed.³⁷

It is possible that improved rf schemes can be developed by optimal control approaches.³⁸ Nevertheless, the results presented here show that the HDR MLEV-32 and HDR WALTZ-32 schemes seem to fulfill the requirements for MQ relaxation studies.

ACKNOWLEDGMENTS

We thank Elodie Salager for her contribution to preliminary studies. This work was supported by the Swiss National Science Foundation (FNSNF), the Swiss Commission for Technology and Innovation (CTI), and the Agence Nationale de la Recherche (ANR) of France (Contract No. NT05-4_43730).

- ¹C. Wang and A. G. Palmer, *Magn. Reson. Chem.* **41**, 866 (2003).
- ²A. Mittermaier and L. E. Kay, *Science* **312**, 224 (2006).
- ³H. Y. Carr and E. M. Purcell, *Phys. Rev.* **94**, 630 (1954).
- ⁴S. Meiboom and D. Gill, *Rev. Sci. Instrum.* **29**, 688 (1958).
- ⁵Z. Luz and S. Meiboom, *J. Chem. Phys.* **39**, 366 (1963).
- ⁶A. G. Palmer III, *Chem. Rev.* **104**, 3623 (2004).
- ⁷C. Deverell, R. E. Morgan, and J. H. Strange, *Mol. Phys.* **18**, 553 (1970).
- ⁸A. Abragam, *Principles of Nuclear Magnetism* (Oxford University Press, Oxford, 1983).
- ⁹H. Desvaux and M. Goldman, *J. Magn. Reson., Ser. B* **110**, 198 (1996).
- ¹⁰I. S. Podkorytov and N. R. Skrynnikov, *J. Magn. Reson.* **169**, 164 (2004).
- ¹¹A. G. Palmer and F. Massi, *Chem. Rev.* **106**, 1700 (2006).
- ¹²O. Millet, J. P. Loria, C. D. Kroenke, M. Pons, and A. G. Palmer, *J. Am. Chem. Soc.* **122**, 2867 (2000).
- ¹³M. Tollinger, N. R. Skrynnikov, F. A. A. Mulder, J. D. Forman-Kay, and L. E. Kay, *J. Am. Chem. Soc.* **123**, 11341 (2001).
- ¹⁴R. Ishima and D. Torchia, *J. Biomol. NMR* **25**, 243 (2003).
- ¹⁵M. J. Grey, C. Wang, and A. G. Palmer, *J. Am. Chem. Soc.* **125**, 14324 (2003).
- ¹⁶F. Massi, E. Johnson, C. Wang, M. Rance, and A. G. Palmer, *J. Am. Chem. Soc.* **126**, 2247 (2004).
- ¹⁷F. Massi, M. J. Grey, and A. G. Palmer, *Protein Sci.* **14**, 735 (2005).
- ¹⁸V. V. Krishnan and M. Rance, *J. Magn. Reson., Ser. A* **116**, 97 (1995).
- ¹⁹D. F. Hansen, D. Yang, H. Feng, Z. Zhou, S. Wiesner, Y. Bay, and L. E. Kay, *J. Am. Chem. Soc.* **129**, 11468 (2007).
- ²⁰K. Kloiber and R. Konrat, *J. Biomol. NMR* **18**, 33 (2000).
- ²¹D. Früh, J. R. Tolman, G. Bodenhausen, and C. Zwanen, *J. Am. Chem. Soc.* **123**, 4810 (2001).
- ²²J. Dittmer and G. Bodenhausen, *J. Am. Chem. Soc.* **126**, 1314 (2004).
- ²³J. Wist, D. Frueh, J. R. Tolman, and G. Bodenhausen, *J. Biomol. NMR* **28**, 263 (2004).
- ²⁴D. M. Korzhnev, P. Neudecker, A. Mittermaier, V. Y. Orekhov, and L. E. Kay, *J. Am. Chem. Soc.* **127**, 15602 (2005).
- ²⁵M. H. Levitt and R. Freeman, *J. Magn. Reson.* **43**, 502 (1981).
- ²⁶M. H. Levitt, R. Freeman, and T. Frenkiel, *J. Magn. Reson.* **55**, 487 (1983).
- ²⁷M. H. Levitt, *Prog. Nucl. Magn. Reson. Spectrosc.* **18**, 61 (1986).
- ²⁸R. Freeman, *Spin Choreography: Basic Steps in High Resolution NMR* (Oxford University Press, Oxford, 1998).

- ²⁹ A. J. Shaka, J. Keeler, T. Frenkiel, and R. Freeman, *J. Magn. Reson.* **52**, 335 (1983).
- ³⁰ W. Magnus, *Commun. Pure Appl. Math.* **7**, 649 (1954).
- ³¹ U. Haeberlen and J. S. Waugh, *Phys. Rev.* **175**, 453 (1968).
- ³² M. H. Levitt, *J. Chem. Phys.* **128**, 052205 (2008).
- ³³ M. Guenneugues, P. Berthault, and H. Desvaux, *J. Magn. Reson.* **136**, 118 (1999).
- ³⁴ A. J. Shaka, P. B. Barker, and R. Freeman, *J. Magn. Reson.* **64**, 547 (1985).
- ³⁵ A. J. Shaka, C. J. Lee, and A. Pines, *J. Magn. Reson.* **77**, 274 (1988).
- ³⁶ T. Gullion, D. B. Baker, and M. S. Conradi, *J. Magn. Reson.* **89**, 479 (1990).
- ³⁷ P. Pelupessy, G. M. Espallargas, and G. Bodenhausen, *J. Magn. Reson.* **161**, 258 (2003).
- ³⁸ N. Khaneja, R. Brockett, and S. J. Glaser, *Phys. Rev. A* **63**, 032308 (2001).